Journal of Animal & Plant Sciences, 36(1): 2026, Page: 227-236
ISSN (print): 1018-7081; ISSN (online): 2309-8694
https://doi.org/10.36899/JAPS.2026.1.0019

MECHANISM OF BEVACIZUMAB REGULATING JAK2/STAT3 PATHWAY TO INHIBIT ANGIOGENESIS IN MICE WITH OVARIAN CANCER

C.Y. Zhang[1#], Z.E. Zhang[2#] and S.R. Zhang[2*]

[1]Department of Gynaecology, Jingzhou Maternal and Child Health Hospital, Jingzhou 434020, Hubei, China;
[2]Gynecology Second Ward, Jingzhou Central Hospital & Jingzhou Hospital, Yangtze University, Jingzhou 434020, China.
#These authors contributed equally to this work.
*Corresponding author's Email: zhangshuirongtze@163.com

ABSTRACT

This study aimed to demonstrate the mechanism of bevacizumab in inhibiting angiogenesis in mice with ovarian cancer (OC) by regulating JAK2/STAT3 pathway. Forty healthy female BALB/C nude mice were randomly assigned to control, model, erlotinib, and bevacizumab groups. Control group received no treatment. Model group received subcutaneous injection in the left axillary region to establish the OC model and received an equal volume of normal saline. Bevacizumab group underwent the same model - establishment procedure and then received 5mg/kg bevacizumab intervention. Erlotinib group also underwent model establishment and received 30 mg/kg erlotinib intervention. Tumor tissue mass and tumor inhibition rate were recorded. The tumor pathological changes were analyzed by hematoxylin-eosin (HE) staining. The microvessel density (MVD) and vascular endothelial growth factor (VEGF) protein expression in tumor tissues were subjected to detection by immunohistochemistry. The expression of JAK2, STAT3, and VEGF in tumor tissues was analyzed using RT-qPCR and western blotting. Compared with the model group, tumor volume and weight of OC in erlotinib group and bevacizumab group of mice were visibly reduced. MVD, JAK2, STAT3, and VEGF in model, erlotinib, and bevacizumab groups of mice were increased versus control, while those were decreased in erlotinib and bevacizumab groups of mice versus model group ($P < 0.05$). Bevacizumab effectively suppressing tumor growth by reducing tumor angiogenesis and reducing the expression of key molecules of JAK2/STAT3 pathway in mice.

Keywords: bevacizumab; ovarian cancer; JAK2/STAT3 pathway; tumor angiogenesis

Published first online December 05, 2025 Published final January 20, 2026

INTRODUCTION

Ovarian cancer (OC) is difficult to treat with a poor prognosis. Treatment effect for metastatic OC is still not ideal (Shaik *et al.,* 2021; Stewart and Lockwood, 2019). OC's malignant progression and treatment resistance are related to angiogenesis in tumor microenvironment (TME) (Lheureux *et al.,* 2019; Nebgen *et al.,* 2019). Elevated vascular endothelial growth factor (VEGF) and its receptor (VEGFR) are associated with the severity and prognostic outcomes of OC (Kuroki *et al.,* 2022). Bevacizumab acts through specific binding with VEGF, thus blocking the interaction between VEGF and its receptor. This effect inhibits the proliferation, migration and survival of endothelial cells, and ultimately tumor angiogenesis (Li *et al.,* 2024a). It was proved effective in treating various malignant tumors (Garcia *et al.,* 2020). It was also reported that bevacizumab plus chemotherapy greatly enhances progression-free survival compared to chemotherapy alone (Zheng *et al.,* 2023). Bevacizumab inhibits OC cell growth and transplanted tumors (Fan *et al.,* 2022). However, mechanism of bevacizumab remains unclear, and other pathways may be involved.

JAK2/STAT3 pathway is involved in regulating cell proliferation, differentiation, survival, and angiogenesis (Gai *et al.,* 2024). It is often abnormally activated, promoting tumor cell growth, survival, and angiogenesis (Li *et al.,* 2024b). JAK2/STAT3 pathway's activation is associated with the progression of OC. Inhibition of this pathway can suppress OC cell proliferation, induce cell apoptosis, and reduce tumor angiogenesis (Gritsina *et al.,* 2015). Hence, JAK2/STAT3 pathway may represent a potential target for bevacizumab's anti-angiogenic effects.

To demonstrate the mechanism of bevacizumab inhibiting OC angiogenesis, we established an OC mouse model. Human OC cell lines were inoculated into immunodeficient mice to simulate human OC. This study aimed to reveal the specific mechanism through which bevacizumab regulates JAK2/STAT3 pathway to inhibit OC angiogenesis by analyzing impact of bevacizumab on

tumor growth, angiogenesis, and JAK2/STAT3 pathway. This research sought to provide a new theoretical basis for anti-angiogenic therapy in OC.

MATERIALS AND METHODS

Animals and grouping: Forty healthy female BALB/C nude mice (4-5 weeks, 22-27 (average: 25.33±2.06) g, Chengdu Dossy Experimental Animals, China) were housed in SPF-grade experimental animal rooms, under environmental conditions, with the temperature meticulously regulated to a range of (25±2) **°C** and the relative humidity maintained between 45% and 50%. This stable environment was complemented by a consistent 12-h light-dark cycle, designed to mimic natural day-night patterns and promote physiological rhythms within the animals. The mice were provided with unrestricted access to water and food. All animal experiments were approved by Ethics Committee of Jingzhou Maternal and Child Health Hospital, according to Chinese national guidelines for the care and use of animals.

Two weeks later, all mice were randomly assigned to control, model, erlotinib, and bevacizumab groups (n=10). Control group served as the untreated control, model group was established using a subcutaneous injection in the left axillary region for the OC model, bevacizumab group was treated with 5 mg/kg bevacizumab after model establishment, erlotinib group was treated with 30 mg/kg erlotinib after model establishment, and model group was given an equal volume of physiological saline.

Animal model establishment: SKOV-3 in good growth condition was cultured until the cell density exceeded 90%. SKOV-3 was digested, and centrifugation was carried out at 1,000 rpm in a short time. The phosphate buffered saline (PBS) buffer was applied, and SKOV-3 was adjusted to 1×10^7/mL. 0.1 mL suspension was administered via subcutaneous injection into the armpit of the left upper limb of BALB/c nude mice to establish the model. Two weeks after modeling, the growth of the tumor mass at the subcutaneous transplantation site was observed, and the model was considered successful when the tumor diameter reached 3mm.

When tumor volume reached 100 mm^3, mice were treated accordingly. Model group received physiological saline, 0.2 mL per intraperitoneal injection, twice daily; bevacizumab group received 5 mg/kg bevacizumab, 0.1 mL per intraperitoneal injection, once daily. Erlotinib group received an intraperitoneal injection of 30mg/kg erlotinib (Roche, Switzerland), 0.1 mL per injection, once daily. The treatment was continued for 3 weeks, and the food and water intake of the nude mice were observed daily.

Measurement of OC tumor indices: The tumor length and width were measured every two days using a vernier caliper (Shanghai Huiyi Ruler Co., Ltd., China) after the model was established, and the volumetric assessment of the tumors was meticulously conducted. Following a period of 28 days post the establishment of the model, the mice were subjected to a humane endpoint through cervical dislocation. The tumor tissues were meticulously excised, ensuring careful handling to avoid any contamination or damage that could affect subsequent analyses. The excised tumor tissues were then subjected to gravimetric measurement, with their weight being precisely determined to calculate the tumor inhibition rate.

HE staining analysis of tumor pathological changes: Twenty-four hours after the final treatment, the tumor tissue of the dead mice was collected. A portion of the tissue was fixed in 4% formaldehyde, embedded in paraffin, and sectioned at 4μm. The morphology of the mice tumor tissue was observed. The process began with the deparaffinization of the sections in xylene for 30 min. The sections were hydrated in graded alcohol for 5 min, rinsed in distilled water for 2 min, subjected to staining with hematoxylin (Beyotime Biotechnology, China) in a short time, and rinsed in tap water for 1 min. The differentiation step employed hydrochloric acid ethanol in a 30 s. They were rinsed in tap water for 15 min, subjected to staining with eosin (Beyotime Biotechnology, China) for 2 min, subjected to dehydration in graded alcohol for 5 min, hyalinized in xylene for 5 min, and mounted with neutral resin for observation.

Immunohistochemistry to detect the expression of CD34 and VEGF: Mice OC tissue samples were collected, fixed, and embedded in paraffin, then sectioned into 0.5μm slices. After baking, they were immediately soaked in xylene I and II for 20 min each, and then dehydration was carried out by alcohol liquid with decreasing concentrations (100% alcohol I, II, 95% alcohol I, II, 90%, 80%, 70% alcohol) provided by Tianjin Fuyu Chemical Co., Ltd., China, for 5 min each. Sections were then thoroughly rinsed in double-distilled water, placed in a 3% hydrogen peroxide solution at 25℃ for 15 min, and rinsed twice with PBS for 3 min, respectively. Sections were placed in a citrate retrieval solution and microwaved for 20 min, cooled to 25℃, and rinsed with distilled water and PBS. Primary antibodies for CD34 and VEGF were applied at 1:50, incubation at 37**°C** for 30 min, followed by PBS rinses. A diaminobenzidine chromogen solution from Beijing Zhongshan Biotechnology Co., Ltd., China, was used for the reaction for 3 min, and staining outcomes were examined under a microscope (Olympus, Japan). The sections were rinsed with tap water, counterstained with hematoxylin, differentiated with salt-alcohol, and blued with ammonia water, followed by another dehydration process in alcohol solutions of increasing concentrations

(70%, 80%, 90% alcohol, and 95% alcohol I, II, 100% alcohol I, and II) for 5 min, respectively. Finally, the sections were hyalinized in xylene I and II for 5 min, respectively, mounted, and observed. VEGF expression was comprehensively assessed by combining the intensity of positive expression and the count of positively expressing cells. The microvessel density (MVD) was assessed based on immunohistochemistry results. Five random tissue sections were selected for analysis. The areas of CD34-positive MVD were observed under a 100x microscope and then counted in detail under a 200x microscope. Each yellow-stained endothelial cell or cell cluster having clear boundaries with the surrounding tissue was counted as one vessel. The number of microvessels in each randomly selected field was recorded, and their average value was calculated as the MVD value for each mouse.

RT-qPCR detecting: The RT-qPCR method was adopted. 100 mg of OC tissue were mixed with 1 mL of TRIzol reagent (Invitrogen, USA). The total RNA was extracted after homogenization and detected for purity and concentration using a Qubit fluorometer (Thermo Fisher, USA) and agarose gel electrophoresis. A reverse transcription kit (Thermo Fisher, USA) was employed to synthesize cDNA, with a system of 20 μL:1 μg of RNA, 2 μL of 10 mmol/L dNTP, 4 μL of 5× Buffer, 1 μL of OligodT, and 0.5 μL of reverse transcriptase. The reverse transcription program was 42**℃** for 60 min and 75**℃** for 10 min.

To ensure subsequent RT-PCR amplification accuracy, primer efficiency validation was performed for JAK2, STAT3, VEGF, and β-actin prior to formal experiments. Total RNA was serially diluted into five gradients and reverse transcribed, followed by RT-qPCR amplification using the corresponding primers. Standard curves were generated by plotting the logarithm of template concentration against Ct values. Linear regression analysis demonstrated that all primers exhibited amplification efficiencies between 90%-110%, with correlation coefficients of standard curves exceeding 0.99.

1 μL of the reverse transcription product served as a template for RT-PCR amplification using a RT-qPCR kit (Thermo Fisher, USA) on a RT-qPCR system (Roche, Switzerland): 95**℃** for 3 min, 95**℃** for 10 s, 55**℃** for 34 s, for 30 cycles. β-actin was used for analyzing JAK2, STAT3, and VEGF genes. Each reaction was performed in triplicate, annealing at 60**℃** for 30 s, 30 cycles. Relative expression was computed employing the $2^{-\Delta\Delta ct}$ assay. The primers for *JAK2*, *etc.* were designed and synthesized by Shanghai Sangon Biotech Co., Ltd (China).

RT-qPCR amplification primers: *JAK2* forward primer (F): 5'-GGGTGTTCGCGTCGCCACTT-3', reverse primer (R): 5'-CAGATCGGGCGACCAGAGCG-3'; *STAT3* F: 5'-GCAGTTTCTGGCCCCCCTT-3', R: 5'-CGGGCCACAATCCGGGCAAAT-3'; VEGF F: 5'-GGCCTCCGAAACCATGAACAT-3', R: 5'-GGTCTCGCATTGCGATGGCAGT-3'; *β-actin* F: 5'-GAGCCTCGCTTTTTTGCCGATCC-3', R: 5'-CGATGCCGTTGCTCGATGGGG-3'.

Melting curve analysis was performed following RT-qPCR amplification to verify amplification specificity. The reaction system was gradually heated from 60°**C** to 95°**C** at 0.5°**C**/s, with continuous fluorescence monitoring. A single sharp peak in the melting curve indicated specific amplification of the target product.

Western blotting: JAK2, STAT3, and VEGF play pivotal roles in cellular proliferation and angiogenesis. Meanwhile, GSK-3β and β-catenin, key components of Wnt/β-catenin signaling, are critically involved in cancer stem cell properties and tumor metastasis. To comprehensively investigate the mechanistic roles of these pathways in OC tissues, Western blotting was performed to analyze JAK2, GSK-3β, STAT3, VEGF, and β-catenin protein expression levels. One hundred milligrams of OC tissue minced and homogenized. 1 mL of protein lysis solution (Beyotime Biotechnology, China) was applied for grinding on ice for 30min, and centrifugation was performed at 4**℃** and 12,000 rpm for 20 min to collect the extracted total protein. The content was determined employing a bicinchoninic acid assay kit (Takara, China). Denaturation was carried out by heating in boiling water in a short time. The separation was achieved through SDS-PAGE gel electrophoresis (Beyotime Biotechnology, China). The proteins were transferred to a polyvinylidene fluoride membrane (Thermo Fisher Scientific, USA) adopting a wet transfer method at 250 mA for 60-90 min. 5% skim milk (Bright Dairy & Food Co., Ltd., China) was adopted for blocking for 1 h, incubation throughout the night at 4**℃** with diluted rabbit anti-human JAK2 (1:200), GSK-3β (1:200), STAT3 (1:400), and VEGF primary antibody (1:500) (Abcam, UK). After three-time rinses with TBST, each lasting 10 min, incubation was carried out with HRP-conjugated secondary antibody (1:10,000) (Zhongshan Golden Bridge, USA) at 25℃ for 2 h, three-time rinses (10 min/time). It was then developed with a chromogenic solution and automatically exposed on a film imager (Pharmacia, USA), and expressions of p-GSK-3β, GSK-3β, and β-catenin were analyzed based on the grayscale values.

Statistical methods: The experimental data underwent analysis using *SPSS 26.0*, with the quantitative results being presented as mean ± sd ($\overline{x}$ ± s). One-way analysis of variance and *t*-test were adopted, and the quantitative data with uneven variance was analyzed by non-parametric test. The counting data were denoted as

percentage (%), and χ^2 test was adopted. $P<0.05$ indicated that the distinction was statistically meaningful.

RESULTS

Analysis of tumor indexes of OC: In Figure 1, the weight of OC tumor in erlotinib and bevacizumab groups was found to have decreased versus model group ($P<0.05$). There was no significant difference in tumor inhibition rate between erlotinib and bevacizumab groups ($P>0.05$). Relative to model group, the tumor volume in erlotinib group was significantly reduced at 6 d post-modeling, and the tumor volume in bevacizumab group was also decreased at 8 d post-modeling ($P<0.05$), negligible difference in tumor volume between erlotinib and bevacizumab groups at different time points ($P>0.05$).

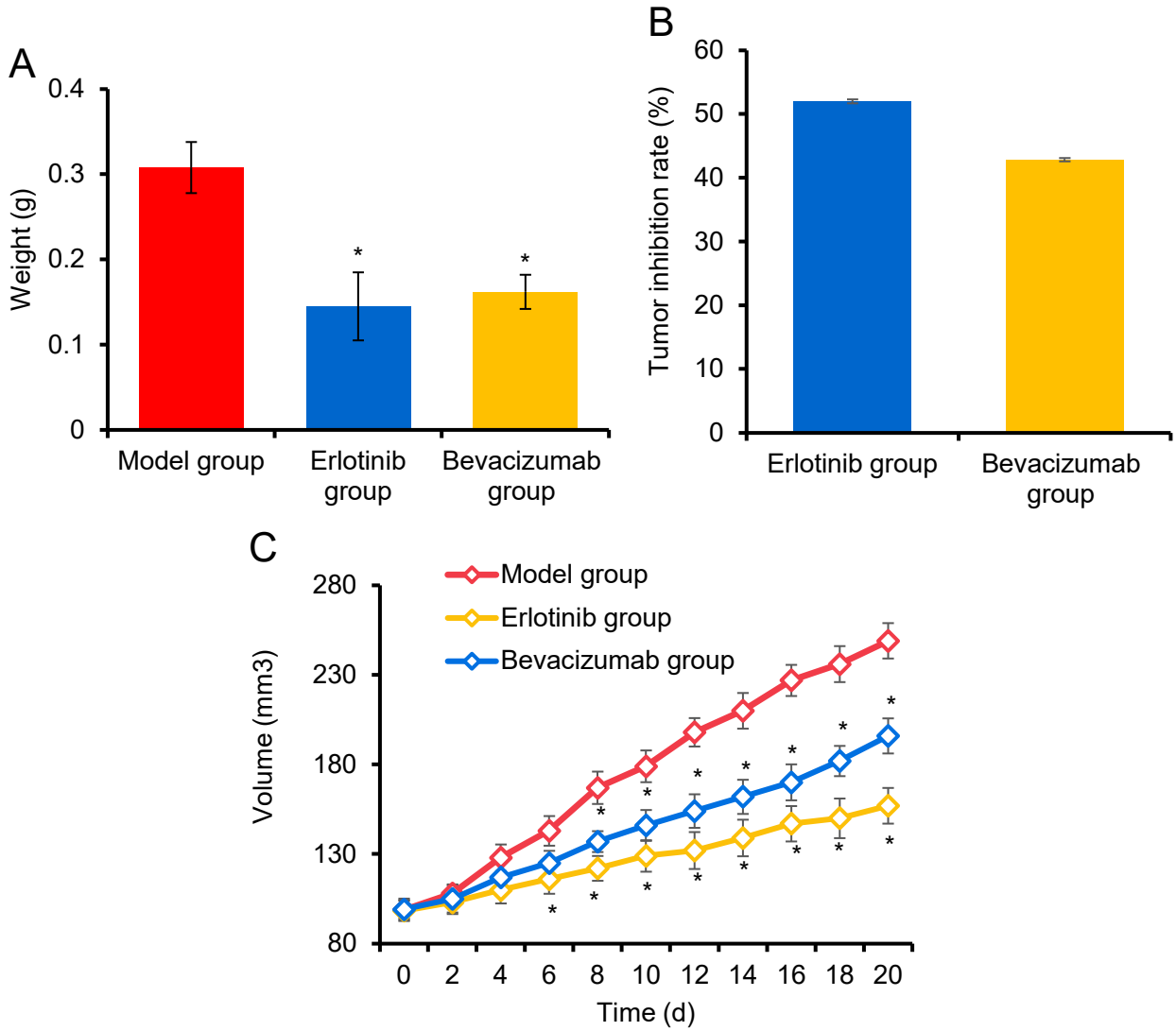

Fig. 1: Comparison of tumor weight, tumor inhibition rate, and tumor volume among different groups of mice. A: weight; B: tumor inhibition rate; C: tumor volume of OC. *$P<0.05$ vs. model group.

Analysis of HE staining results of OC tissues: In control group, OC cells showed normal and clear outline, abundant cytoplasm and obvious nucleoli. There was no obvious cell atypia and the cell morphology was normal. In model group, they indicated island like growth, increased nuclear division, resulting in blurred cell outline, high-density distribution of cancer cells with different size and morphology, and scattered neutrophil infiltration in the stroma; In erlotinib group and bevacizumab group, they indicated shrunken morphology, concentrated nuclear chromatin, and different degrees of patchy necrotic areas (Figure 2).

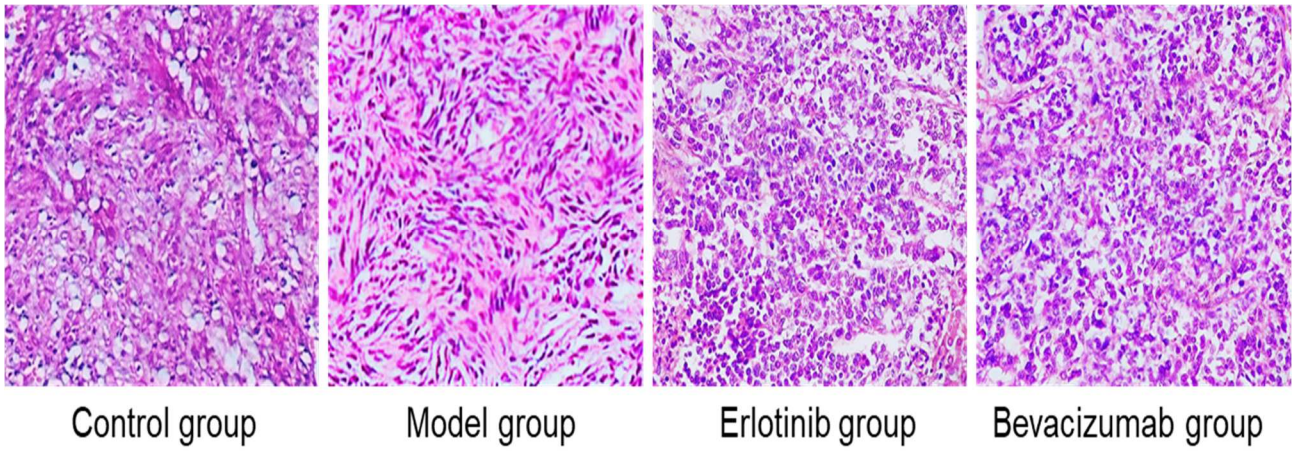

Fig.2: OC tissue HE staining in different groups of mice (×200).

Analysis of immunohistochemical results: In Figure 3, the MVD and VEGF protein expression in model, erlotinib, and bevacizumab groups was increased versus control group. When compared with model group, it was visibly decreased in erlotinib group and bevacizumab group (P<0.05). It showed no significant disparity between erlotinib and bevacizumab groups (P>0.05).

Analysis of gene expression in OC tissues: In Figure 4, JAK2, STAT3, and VEGF gene expressions in model, erlotinib, and bevacizumab groups was visibly increased versus control, while those were reduced in erlotinib and bevacizumab groups versus model group (P<0.05), but exhibited negligible disparity between erlotinib and bevacizumab groups (P>0.05).

Analysis of protein expression in OC tissues: In Figure 5, JAK2, STAT3, and VEGF protein expressions in model group, erlotinib group, and bevacizumab group were markedly elevated versus control; which were markedly reduced in erlotinib and bevacizumab groups versus model group (P<0.05). Negligible difference was observed between erlotinib and bevacizumab groups (P>0.05).

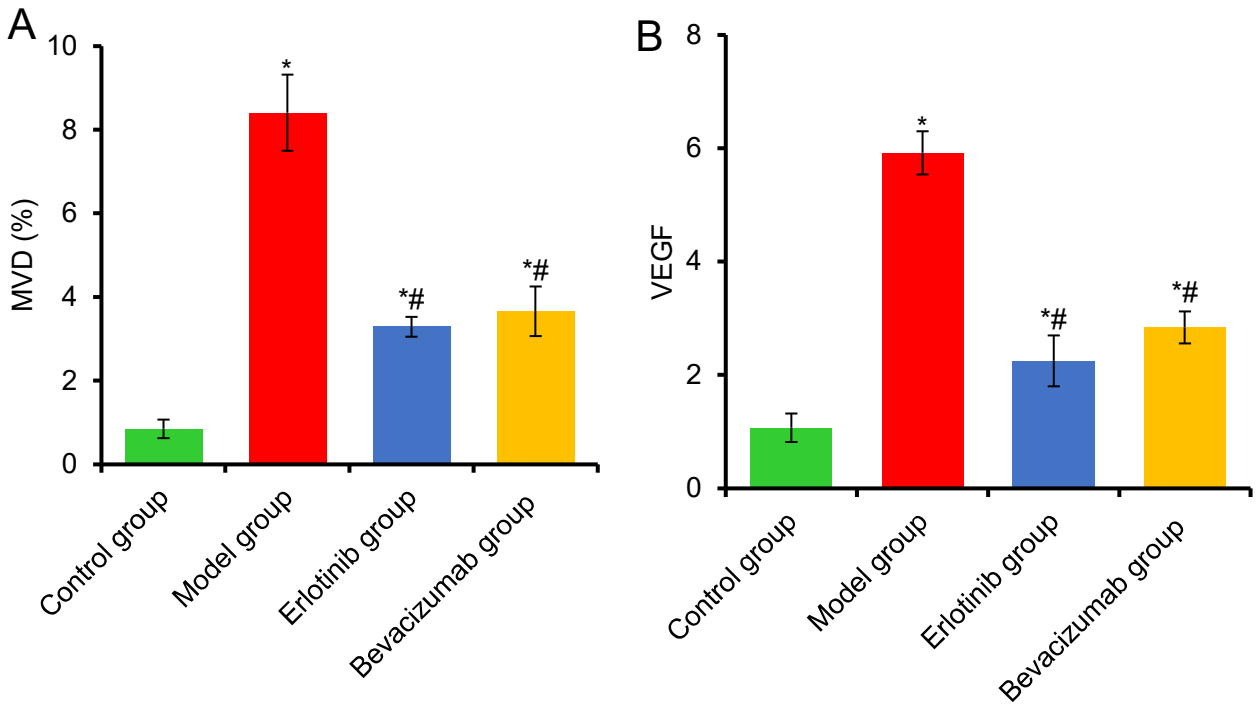

Fig.3: Comparison of MVD and VEGF protein expression levels in OC tissues of different groups of mice detected by immunohistochemistry. A. MVD; B. VEGF.
***P<0.05 vs. control group, $^{\#}P$<0.05 vs. model group.**

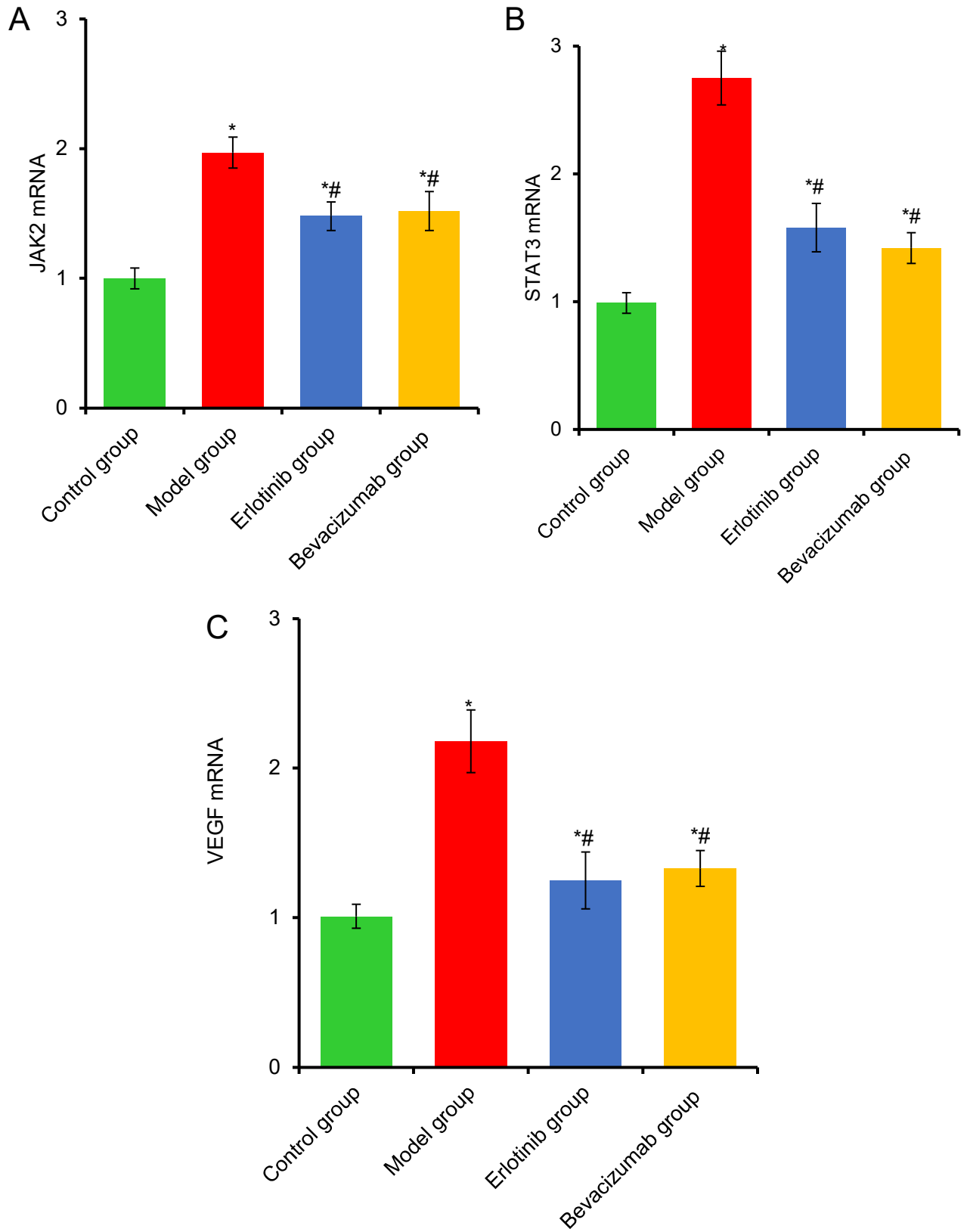

Fig.4: Comparison of gene expression levels in OC tissues of different groups of mice. A. JAK2; B. STAT3; C. VEGF. ****P*<0.05 vs. control group, #*P*<0.05 vs. model group.

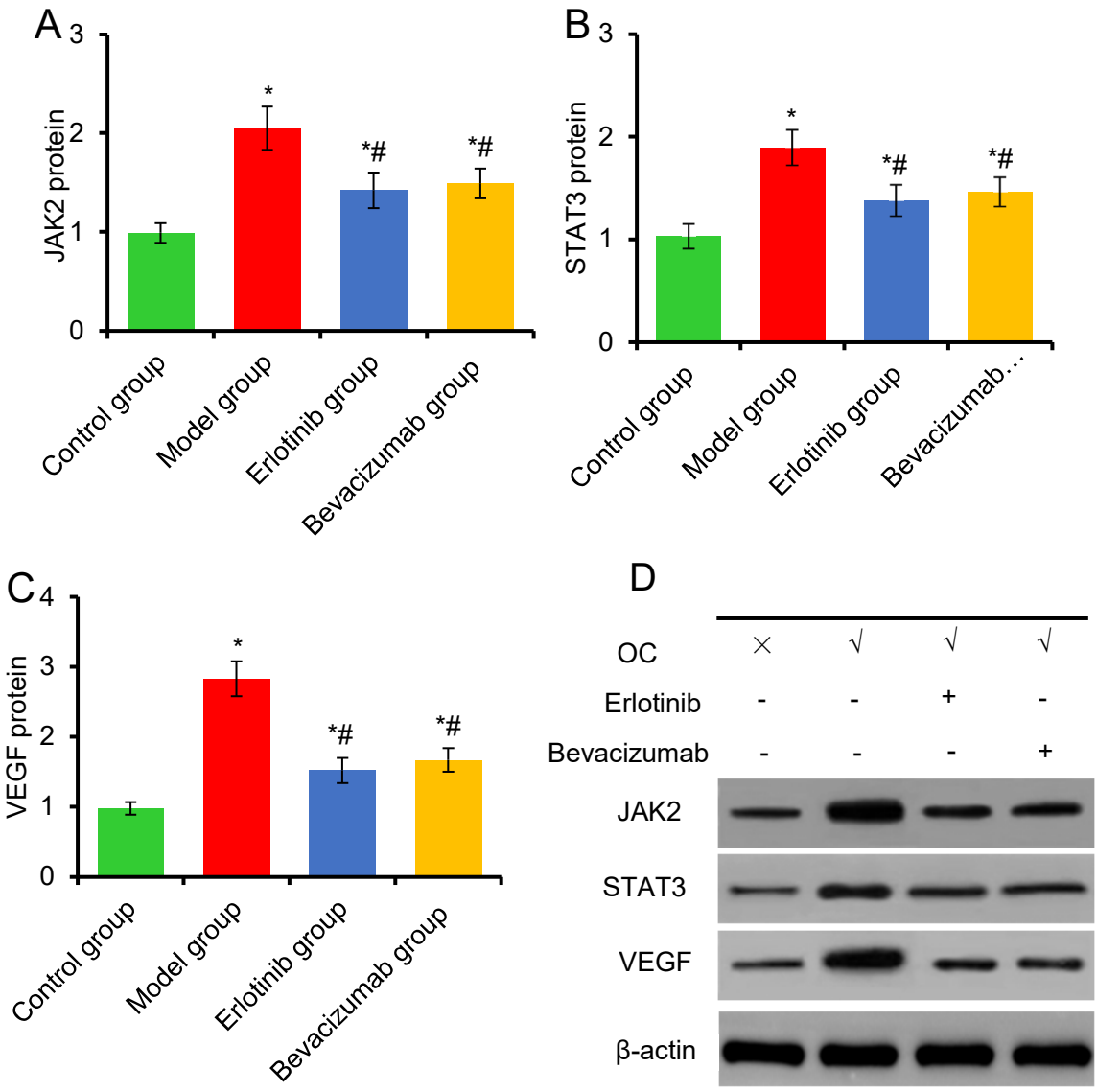

Fig. 5: Comparison of protein expression levels in OC tissues of mice in different groups. A: JAK2; B: STAT3; C: VEGF; D: western blotting. **P*<0.05 vs. control group, #*P*<0.05 vs. model group.

DISCUSSION

In this study, the mechanism of bevacizumab regulating JAK2/STAT3 pathway to inhibit angiogenesis of OC was explored through animal OC model. Contrast with model group showed that the volume and weight of OC markedly reduced in erlotinib group and bevacizumab group, indicating that both drugs effectively inhibited the growth of tumors. The anti-tumor outcome of bevacizumab on OC is equivalent to that of erlotinib, and it plays an effective role in suppressing tumor growth by reducing tumor angiogenesis and downregulating expression of key molecules of JAK2/STAT3. These findings support the potential of bevacizumab as a therapeutic drug for OC and provide an experimental basis for its clinical application.

From the volume and weight data, erlotinib and bevacizumab showed observable impact on suppressing the growth of OC, and this effect shows a similar trend at different time points after modeling. This may be related to their mechanism of action. Erlotinib interferes with tumor cell proliferation and pathways by suppressing tyrosine kinases (Hardesty *et al.,* 2022), while bevacizumab reduces angiogenesis by suppressing VEGF, thereby suppressing tumor growth (Horikawa *et al.,* 2020). Changes in the effects of erlotinib and bevacizumab at different time points also suggest that the effects of drugs may be time-dependent. The tumor volume was markedly reduced in the early stage after

modeling, which may reflect its rapid intervention effect on tumor growth. The above results further suggested that bevacizumab and erlotinib, both positive drugs, suggested good antitumor effects in the treatment of OC.

JAK is a member of a family of non-receptor tyrosine kinases, whose main function is to transmit signals by phosphorylating the substrate STAT (Long *et al.,* 2024). After JAK is activated on cell membrane receptors, it activates STAT molecules through tyrosine phosphorylation, promoting its dimerization and translocation to the nucleus to regulate the transcriptional activity of specific genes (Huang *et al.,* 2022). In many cancers, JAK2/STAT3 is abnormally activated. This abnormal activation is usually achieved by gene mutation, overexpression, or abnormal enhancement of upstream signals (You *et al.,* 2023; Stevens *et al.,* 2023; Lei *et al.,* 2019; Deng *et al.,* 2023). As reported, STAT3 is abnormally activated in cancer cells, promoting proliferation, apoptosis escape, and metastasis of cancer cells (Chen *et al.,* 2023). The abnormal activation of JAK2/STAT3 can foster the abnormal multiplication and neoplastic transformation of tumor cells (Liu *et al.,* 2022). When cancer cells shed, invade, and metastasize, the activation of JAK2/STAT3 accelerates these processes. STAT3 promotes the formation of tumor neovascularization, further supporting tumor spread and growth (Xu *et al.,* 2022). The results showed that the levels of MVD and VEGF protein in model group were markedly superior to those in control group. This shows that tumor angiogenesis in OC model is notably increased. Under hypoxic conditions in the TME, hypoxia-inducible factor-1α (HIF-1α) stabilizes and translocates to the nucleus (Anjum *et al.,* 2022). HIF-1 α binds to hypoxia response elements in the VEGF promoter region, upregulating the transcription and expression of VEGF. VEGF subsequently binds to VEGFRs on endothelial cells, activating pathways that promote endothelial cell proliferation and migration, leading to new blood vessel formation (Wu *et al.,* 2023). Erlotinib and bevacizumab groups showed greatly reduced MVD and VEGF protein expression versus model group. Erlotinib blocks EGFR signaling, thereby suppressing VEGF production and angiogenesis (Rohr-Udilova *et al.,* 2017). Bevacizumab directly neutralizes VEGF and prevents its binding to VEGFRs, inhibiting downstream pathways and effectively suppressing angiogenesis and tumor growth (Butler *et al.,* 2017). In this study, erlotinib and bevacizumab effectively inhibit angiogenesis and VEGF expression in OC. JAK2, STAT3, and VEGF gene expression was markedly increased in model group versus control. JAK2 and STAT3 regulate VEGF expression, affecting angiogenesis and tumor growth (He *et al.,* 2022). As an anti VEGF antibody, bevacizumab directly targets VEGF and prevents its binding with VEGFR, thus suppressing angiogenesis and tumor growth. VEGF can bind to VEGFR, increasing the permeability of blood vessels (Xia *et al.,* 2023). Such effect is imperative for tumor growth and metastasis, for providing blood supply required for tumor growth. VEGF promotes angiogenesis and synthesis and secretion of MMPs (Xiong *et al.,* 2021). The highly expressed VEGF is closely related to the clinical stage, cell differentiation, and lymph node metastasis of tumors (Fogg *et al.,* 2019). Activation of JAK2/STAT3 can enhance VEGF expression, thereby promoting angiogenesis and tumor invasion (Zhong *et al.,* 2021). Elevated VEGF can activate JAK2/STAT3, forming a vicious cycle and promoting tumor progression (Wang *et al.,* 2025). The abnormal activation of this pathway promotes tumor cell growth and metastasis, and aggravates the malignant progression. Hence, JAK2/STAT3 and its downstream effectors demonstrate imperative targets in cancer therapy.

In this study, it was found that bevacizumab effectively inhibited tumor growth by reducing tumor angiogenesis and reducing JAK2/STAT3 key molecule expression. Although JAK2, STAT3, and VEGF levels were analyzed, this work did not explore the specific interaction between these molecules or other possible downstream effects, and did not evaluate other involved pathways. We will explore mechanism of JAK2/STAT3 and evaluate the impact of other possible pathways on the therapeutic effect.

Conclusion: This study explored the mechanism by which bevacizumab regulates the JAK2/STAT3 pathway and inhibits angiogenesis in OC mice. It turned out that bevacizumab inhibited tumor growth by reducing tumor angiogenesis and reducing JAK2/STAT3 key molecule expression, offering robust justification for the utilization of bevacizumab in OC treatment. This study helps to develop OC treatment plans, discover new drug targets, and improve the accuracy of treatment efficacy prediction.

Authors' Contribution: Conception and design: Chongyuan Zhang, Zheng'e Zhang and Shuirong Zhang; Administrative support: Shuirong Zhang; Provision of study materials: Shuirong Zhang; Collection and assembly of data: Chongyuan Zhang and Zheng'e Zhang; Data analysis and interpretation: Chongyuan Zhang and Zheng'e Zhang; Manuscript writing: All authors; Final approval of manuscript: All authors.

Competing Interest: The author has declared that no competing interest exists.

Data Availability: All relevant data are within the paper and its supporting information files.

REFERENCES

Anjum, S., S. Sen, K. Chosdol, S. Bakhshi, S. Kashyap, N.Pushker, M. S. Bajaj, R. Meel and M. C. Sharma (2022). Vascular endothelial growth

factor (VEGF) and hypoxia inducible factor-1 alpha (HIF-1α) in lacrimal gland Adenoid cystic carcinoma: Correlation with clinical outcome. Ann Diagn Pathol 56: 151846. https://doi.org/10.1016/j.anndiagpath.2021.151846

Butler, C. T., A. L. Reynolds, M. Tosetto, E. T. Dillon, P. J. Guiry, G. Cagney, J. O'Sullivan and B. N. Kennedy (2017). A Quininib Analogue and Cysteinyl Leukotriene Receptor Antagonist Inhibits Vascular Endothelial Growth Factor (VEGF)-independent Angiogenesis and Exerts an Additive Antiangiogenic Response with Bevacizumab. J Biol Chem. 292(9): 3552-3567. https://doi.org/10.1074/jbc.M116.747766

Chen, H., S. Ren, H. Wan, W. Wei, Y. Luo and M. Cai (2023). DUSP1 regulates the JAK2/STAT3 signaling pathway through targeting miR-21 in cervical cancer cells. Cell Mol Biol 69: 40-44. https://doi.org/10.14715/cmb/2023.69.8.6

Deng, H., X. Gong, G. Ji, C. Li and S. Cheng (2023). KIF2C promotes clear cell renal cell carcinoma progression via activating JAK2/STAT3 signaling pathway. Mol Cell Probes 72: 101938. https://doi.org/10.1016/j.mcp.2023.101938

Fan, Y., H. Cheng, Y. Liu, S. Liu, S. Lowe, Y. Li, R. Bentley, B. King, J.P.W. Tuason, Q. Zhou, C. Sun and H. Zhang (2022). Metformin anticancer: Reverses tumor hypoxia induced by bevacizumab and reduces the expression of cancer stem cell markers CD44/CD117 in human ovarian cancer SKOV3 cells. Front Pharmacol 13: 955984. https://doi.org/10.3389/fphar.2022.955984

Fogg, K.C., W.R. Olson, J.N. Miller, A. Khan, C. Renner, I. Hale, P.S. Weisman and P.K. Kreeger (2019). Alternatively activated macrophage-derived secretome stimulates ovarian cancer spheroid spreading through a JAK2/STAT3 pathway. Cancer Lett 458: 92-101. https://doi.org/10.1016/j.canlet.2019.05.029

Gai, M., L. Zhao, H. Li, G. Jin, W. Li, F. Wang and M. Liu (2024). LCP1 promotes ovarian cancer cell resistance to olaparib by activating the JAK2/STAT3 signalling pathway. Cancer Biol Ther 25(1): 2432117. https://doi.org/10.1080/15384047.2024.2432117

Garcia, J., H.I. Hurwitz, A.B. Sandler, D. Miles, R.L. Coleman, R. Deurloo and O.L. Chinot (2020). Bevacizumab (Avastin®) in cancer treatment: A review of 15 years of clinical experience and future outlook. Cancer Treat Rev 86: 102017. https://doi.org/10.1016/j.ctrv.2020.102017

Gritsina, G., F. Xiao, S.W. O'Brien, R. Gabbasov, M.A. Maglaty, R.H. Xu, R.J. Thapa, Y. Zhou, E. Nicolas, S. Litwin, S. Balachandran, L.J. Sigal, D. Huszar and D.C. Connolly (2015). Targeted Blockade of JAK/STAT3 Signaling Inhibits Ovarian Carcinoma Growth. Mol Cancer Ther 14(4): 1035-47. https://doi.org/10.1158/1535-7163.MCT-14-0800

Hardesty, M.M., T.C. Krivak, G.S. Wright, E. Hamilton, E.L. Fleming, J. Belotte, E.K. Keeton, P. Wang, D. Gupta, A. Clements, H.J. Gray, G.E. Konecny, R.G. Moore and D.L. Richardson (2022). OVARIO phase II trial of combination niraparib plus bevacizumab maintenance therapy in advanced ovarian cancer following first-line platinum-based chemotherapy with bevacizumab. Gynecol Oncol 166: 219-229. https://doi.org/10.1016/j.ygyno.2022.05.020

He, S.L., X. Zhao and S.J. Yi (2022). CircAHNAK upregulates EIF2B5 expression to inhibit the progression of ovarian cancer by modulating the JAK2/STAT3 signaling pathway. Carcinogenesis 43: 941-955. https://doi.org/10.1093/carcin/bgac053

Horikawa, N., K. Abiko, N. Matsumura, T. Baba, J. Hamanishi, K. Yamaguchi, R. Murakami, M. Taki, M. Ukita, Y. Hosoe, M. Koshiyama, I. Konishi and M. Mandai (2020). Anti-VEGF therapy resistance in ovarian cancer is caused by GM-CSF-induced myeloid-derived suppressor cell recruitment. Br J Cancer 122: 778-788. https://doi.org/10.1038/s41416-019-0725-x

Huang, B., X. Lang and X. Li (2022). The role of IL-6/JAK2/STAT3 signaling pathway in cancers. Front Oncol 12:1023177. https://doi.org/10.3389/fonc.2022.1023177

Kuroki, L., S.R. Guntupalli (2022). Treatment of epithelial ovarian cancer. BMJ 371: m3773. https://doi.org/10.1136/bmj.m3773

Lei, T., S. Zhou, Q. Meng and M. Zhang (2019). STAT3 signaling pathway in drug - resistant bladder cancer cell line. J Biol Regul Homeost Agents 33: 1347-1357. https://doi.org/10.23812/19 - 68 - A

Lheureux, S., M. Braunstein and A.M. Oza (2019). Epithelial ovarian cancer: Evolution of management in the era of precision medicine. CA Cancer J Clin 69: 280-304. https://doi.org/10.3322/caac.21559

Li, W., C. Zhou, L. Yu, Z. Hou, H. Liu, L. Kong, Y. Xu, J. He, J. Lan, Q. Ou, Y. Fang, Z. Lu, X. Wu, Z. Pan, J. Peng and J. Lin (2024a). Tumor - derived lactate promotes resistance to bevacizumab treatment by facilitating autophagy enhancer protein RUBCNL expression through histone H3 lysine 18 lactylation (H3K18la) in colorectal cancer. Autophagy 20: 114-130. https://doi.org/10.1080/15548627.2023.2249762

Li, Y.K., A.B. Gao, T. Zeng, D. Liu, Q.F. Zhang, X.M.

Ran, Z.Z. Tang, Y. Li, J. Liu, T. Zhang, G.Q. Shi, W.C. Zhou, W.D. Zou, J. Peng, J. Zhang, H. Li and J. Zou (2024b). ANGPTL4 accelerates ovarian serous cystadenocarcinoma carcinogenesis and angiogenesis in the tumor microenvironment by activating the JAK2/STAT3 pathway and interacting with ESM1. J Transl Med 22(1): 46. https://doi.org/10.1186/s12967-023-04819-8

Liu, M., H. Li, H. Zhang, H. Zhou, T. Jiao, M. Feng, F. Na, M. Sun, M. Zhao, L. Xue and L. Xu (2022). RBMS1 promotes gastric cancer metastasis through autocrine IL-6/JAK2/STAT3 signaling. Cell Death Dis 13: 287. https://doi.org/10.1038/s41419-022-04747-3

Long, L., X. Fei, L. Chen, L. Yao and X. Lei (2024). Potential therapeutic targets of the JAK2/STAT3 signaling pathway in triple-negative breast cancer. Front Oncol 14: 1381251. https://doi.org/10.3389/fonc.2024.1381251

Nebgen, D.R., K.H. Lu and R.C. Bast Jr (2019). Novel Approaches to Ovarian Cancer Screening. Curr Oncol Rep 21: 75. https://doi.org/10.1007/s11912-019-0816-0

Rohr-Udilova, N., F. Klinglmüller, M. Seif, H. Hayden, M. Bilban, M. Pinter, K. Stolze, W. Sieghart, M. Peck-Radosavljevic and M. Trauner (2017). Oxidative stress mediates an increased formation of vascular endothelial growth factor in human hepatocarcinoma cells exposed to erlotinib. Oncotarget. 8(34): 57109-57120. https://doi.org/10.18632/oncotarget.19055

Shaik, B., T. Zafar, K. Balasubramanian and S.P. Gupta (2021). An Overview of Ovarian Cancer: Molecular Processes Involved and Development of Target-based Chemotherapeutics. Curr Top Med Chem 21(4): 329-346. https://doi.org/10.2174/1568026620999201111155426

Stevens, L.E., G. Peluffo, X. Qiu, D. Temko, A. Fassl, Z. Li, A. Trinh, M. Seehawer, B. Jovanović, M. Alečković, C.M. Wilde, R.C. Geck, S. Shu, N.L. Kingston, N.W. Harper, V. Almendro, A.L. Pyke, S.B. Egri, M. Papanastasiou, K. Clement, N. Zhou, S. Walker, J. Salas, S.Y. Park, D.A. Frank, A. Meissner, J.D. Jaffe, P. Sicinski, A. Toker, F. Michor, H.W. Long, B.A. Overmoyer and K. Polyak (2023). JAK-STAT Signaling in Inflammatory Breast Cancer Enables Chemotherapy-Resistant Cell States. Cancer Res 83: 264-284. https://doi.org/10.1158/0008-5472.CAN-22-0423

Stewart, C., C. Ralyea and S. Lockwood (2019). Ovarian Cancer: An Integrated Review. Semin Oncol Nurs 35: 151-156. https://doi.org/10.1016/j.soncn.2019.02.001

Wang, D., L. Li, Y. Zhang and K. Ye (2025). Lipopolysaccharide-Educated Cancer-Associated Fibroblasts Facilitate Malignant Progression of Ovarian Cancer Cells via the NF-kB/IL-6/JAK2 Signal Transduction. Mol Biotechnol 67(1): 317-328. https://10.1007/s12033-024-01055-3

Wu, L., C. Qian, W. Zhang, M. Shi, X. Chen, Y. Wang and F. Lin (2023). Ginkgetin suppresses ovarian cancer growth through inhibition of JAK2/STAT3 and MAPKs signaling pathways. Phytomedicine 116: 154846. https://doi.org/10.1016/j.phymed.2023.154846

Xia, D., X. Xu, J. Wei, W. Wang, J. Xiong, Q. Tan, P. Xue and H. Wang (2023). CHAF1A promotes the proliferation and growth of epithelial ovarian cancer cells by affecting the phosphorylation of JAK2/STAT3 signaling pathway. Biochem Biophys Rep 35: 101522. https://doi.org/10.1016/j.bbrep.2023.101522

Xiong, C., B. Yan, S. Xia, F. Yu, J. Zhao and H. Bai (2021). Tilianin inhibits the human ovarian cancer (PA-1) cell proliferation via blocking cell cycle, inducing apoptosis and inhibiting JAK2/STAT3 signaling pathway. Saudi J Biol Sci 28: 4900-4907. https://doi.org/10.1016/j.sjbs.2021.06.033

Xu, M., L. Ren, J. Fan, L. Huang, L. Zhou, X. Li and X. Ye (2022). Berberine inhibits gastric cancer development and progression by regulating the JAK2/STAT3 pathway and downregulating IL-6. Life Sci 290: 120266. https://doi.org/10.1016/j.lfs.2021.120266

You, Y., X. Chen, X. Chen, H. Li, R. Zhou, J. Zhou, M. Chen, B. Peng, S. Ji, H.Y. Kwan, L. Zou, J. Yu, Y. Liu, Y. Wu and X. Zhao (2023). Jiawei Yanghe Decoction suppresses breast cancer by regulating immune responses via JAK2/STAT3 signaling pathway. J Ethnopharmacol 316: 116358. https://doi.org/10.1016/ j.jep.2023.116358

Zheng, Y., R. Zhou, J. Cai, N. Yang, Z. Wen, Z. Zhang, H. Sun, G. Huang, Y. Guan, N. Huang, M. Shi, Y. Liao, J. Bin and W. Liao (2023). Matrix Stiffness Triggers Lipid Metabolic Cross-talk between Tumor and Stromal Cells to Mediate Bevacizumab Resistance in Colorectal Cancer Liver Metastases. Cancer Res 83: 3577-3592. https://doi.org/10.1158/0008-5472.CAN-23-0025

Zhong, Y., F. Le, J. Cheng, C. Luo, X. Zhang, X. Wu, F. Xu, Q. Zuo and B. Tan (2021). Triptolide inhibits JAK2/STAT3 signaling and induces lethal autophagy through ROS generation in cisplatin resistant SKOV3/DDP ovarian cancer cells. Oncol Rep 45: 69. https://doi.org/10.3892/or.2021.8020.